Published in: *Int'l J. for Numerical Methods in Engg.* 122:21, Nov. 2021, 6341-6360.
https://doi.org/10.1002/nme.6794

A compact three-dimensional fourth order scheme for elasticity using the first-order formulation

Rachel Gordon* Eli Turkel† Dan Gordon‡

Abstract

We develop a compact fourth order scheme for the three-dimensional elastic wave equation in frequency space, using the first order velocity-stress formulation. The scheme is implemented numerically for homogeneous media on a staggered grid, and both the acoustic and elastic cases are considered. We use a one-directional point source of impact, for which Pilant developed a closed solution. Numerical results for the acoustic and the elastic cases compare favorably with the analytic solutions and show a very significant improvement over the second order scheme.

Keywords: Compact schemes; Elastic wave equation; First-order formulation; Fourth order accuracy; Frequency space; Staggered grid.

1 Introduction

In this paper we consider finite difference approximations to the acoustic and elastic wave equations. The acoustic equations apply mainly in air and other simple media. However, when considering waves in a solid it is necessary to account for the elastic (or even visco-elastic) properties of the media. Thus, for example, applications to aerodynamics rely on the wave equation (or their extension to the Euler and Navier-Stokes equations) while applications to seismology rely mainly on the elastic wave equations. These equations are time dependent, but in many applications there is a dominant frequency, so it is appropriate to consider a Fourier transform which transforms the time dependent equations to the frequency domain. We shall develop a compact fourth order scheme for the elastic wave equation in the frequency domain.

There are many reasons to study the elastic wave equations. Seismic waves are caused by earthquakes, volcanic events, and man-made explosions on or below the surface. Another cause

*Department of Aerospace Engineering, the Technion–Israel Inst. of Technology, Haifa 32000, Israel.
rgordon@technion.ac.il
†School of Mathematical Sciences, Tel Aviv University, Tel Aviv 69978, Israel.
turkel@tauex.tau.ac.il
‡Department of Computer Science, University of Haifa, Haifa 34988, Israel.
gordon@cs.haifa.ac.il

for their study is known as "exploration geophysics"; see, for example, Virieux and Operto [33] and Virieux et al. [34]. More details on this topic appear towards the end of this section.

Compact schemes are advantageous for high order schemes in wave equations for three main reasons: (a) in heterogeneous media, the derivatives of the media parameters are localized, and so they are more accurate at each spatial point; (b) they are simpler to handle at the boundaries of the domain; (c) for parallel processing of very large 3D domains, it is necessary to subdivide the domain for parallel processing and compact schemes are much simpler to use at subdomain boundaries.

High order accuracy is important in two distinct applications. Firstly, for a given number of grid points we obtain improved accuracy. Secondly, in three dimensional applications, a very large grid is necessary to achieve a fixed accuracy. This grid may exceed the capabilities of the computer both in terms of computer memory and CPU time. Using a high order method allows us to achieve the same accuracy with a coarser grid. Additionally, in many methods for inverse problems, it is necessary to solve a linear system many times. Hence, it is important to improve the efficiency of the solver, and this can be done by improving the accuracy and reducing the required grid size. We note also that due to the pollution effect [2, 4], the number of grid points per side N required to obtain a given accuracy is governed by the equation $N = Ck^{(p+1)/p}$, where C is a constant, k is the (non-dimensional) wave number, and p is the order of the accuracy of the scheme.

In this paper we develop a compact fourth-order scheme for the elastic wave equation in frequency space, using the first order (velocity-stress) formulation. For the experimental results, we implement our scheme in homogeneous media and compare the results with Pilant's solution – see [23, §7.4]. We also compare the acoustic case with the Green's function solution.

The elastic equations in the time domain can be written both as a system of second order partial differential equations for the displacements (u, v, w) or as a first order system for the displacements and stresses. Note that u, v, w are the displacements in the x, y, z directions, respectively. In the frequency domain, the displacements are replaced by the velocities, which, for convenience, we also refer to them as (u, v, w). The second order system in the frequency domain consists of three equations, one for each component. The equation for u is given by

$$-\rho\omega^2 u = \partial_x \left[\lambda D + 2\mu \frac{\partial u}{\partial x}\right] + \partial_y \left[\mu(\frac{\partial u}{\partial y} + \frac{\partial v}{\partial x})\right] + \partial_z \left[\mu(\frac{\partial u}{\partial z} + \frac{\partial w}{\partial x})\right] + F^u(x, y, z), \quad (1)$$

where ρ is the density, $\omega = 2\pi f$ is the angular frequency, f is the frequency, λ and μ are the Lamé parameters, F^u is the forcing term in the x-direction, and D is the divergence of the velocity vector (u, v, w):

$$D = \frac{\partial u}{\partial x} + \frac{\partial v}{\partial y} + \frac{\partial w}{\partial z}.$$

For an explanation of the elastic wave equation and the physical meaning of the parameters, see, for example, Pilant [23] and Pujol [24]. Virieux [32] introduced a fourth order accurate scheme for the elastic wave equation, using the first order formulation which involves both the velocities and stresses on a non-compact staggered stencil. Fourth order non-compact schemes for these equations in the second order formulation have also been developed, see Nilsson et al. [22], and Sjögreen and Petersson [26]. Komatitisch and Tromp [17] used the spectral element method in which a different discretization stencil is used at each interior node point in each element, even on a regular Cartesian grid. In this paper, we introduce a compact fourth-order scheme using the first order formulation.

In the first order formulation of the elastic wave equation, we have, in addition to the three velocities (u, v, w), six additional stress terms σ_{ij}, $1 \le i, j \le 3$, which form a symmetric matrix. Due to the symmetry, there are only six different values of σ_{ij}, so for $j > i$, we replace σ_{ji} by σ_{ij}. In the following, $D = \frac{\partial u}{\partial x} + \frac{\partial v}{\partial y} + \frac{\partial w}{\partial z}$, and the forcing terms in the x, y, z directions are denoted, respectively, by F^u, F^v, F^w. Then the system is given by

$$-\rho i\omega u = \frac{\partial \sigma_{11}}{\partial x} + \frac{\partial \sigma_{12}}{\partial y} + \frac{\partial \sigma_{13}}{\partial z} + F^u(x, y, z) \tag{2a}$$

$$-\rho i\omega v = \frac{\partial \sigma_{12}}{\partial x} + \frac{\partial \sigma_{22}}{\partial y} + \frac{\partial \sigma_{23}}{\partial z} + F^v(x, y, z) \tag{2b}$$

$$-\rho i\omega w = \frac{\partial \sigma_{13}}{\partial x} + \frac{\partial \sigma_{23}}{\partial y} + \frac{\partial \sigma_{33}}{\partial z} + F^w(x, y, z) \tag{2c}$$

$$-i\omega\sigma_{11} = \lambda D + 2\mu \frac{\partial u}{\partial x} \tag{2d}$$

$$-i\omega\sigma_{22} = \lambda D + 2\mu \frac{\partial v}{\partial y} \tag{2e}$$

$$-i\omega\sigma_{33} = \lambda D + 2\mu \frac{\partial w}{\partial z} \tag{2f}$$

$$-i\omega\sigma_{12} = \mu(\frac{\partial u}{\partial y} + \frac{\partial v}{\partial x}) \tag{2g}$$

$$-i\omega\sigma_{13} = \mu(\frac{\partial u}{\partial z} + \frac{\partial w}{\partial x}) \tag{2h}$$

$$-i\omega\sigma_{23} = \mu(\frac{\partial v}{\partial z} + \frac{\partial w}{\partial y}) \tag{2i}$$

We consider isotropic elasticity and so disturbance to the media causes two types of waves to travel through it: compression, or P waves, and shear, or S waves. The velocities of the P and S waves are denoted, respectively, c_p and c_s. These velocities are related to the Lamé parameters λ and μ as follows:

$$c_p = \sqrt{\frac{\lambda + 2\mu}{\rho}} \qquad \text{speed of the compression or P wave} \tag{3a}$$

$$c_s = \sqrt{\frac{\mu}{\rho}} \qquad \text{speed of the shear or S wave} \tag{3b}$$

The wave numbers associated with the two wave speeds are $k_p = \omega/c_p$ and $k_s = \omega/c_s$.

We note that a staggered grid gives higher accuracy than a non-staggered grid for the same degrees of freedom [29]. Fourth order staggered grid finite difference methods were proposed by Virieux [32], Levander [18], Graves [13] and Li et al. [19,20], and have been used extensively for seismic wave simulations. This method discretizes the elastic wave equation as a first order hyperbolic system using the velocity-stress formulation. For the time domain they achieve only second order accuracy in time. However, their scheme uses a non-compact stencil to achieve the higher accuracy which creates difficulties near boundaries. A spectral discretization in two dimensions was given by Feng et al. [6]. Ma and Ge [21] recently published a compact 4th-order scheme for 2-dimensional elliptic and parabolic equations.

When the parameter c_s is set to zero, equations (2) reduce to the so-called acoustic case, in which $\sigma_{ij} = 0$ for $i \neq j$ and σ_{ii} are all equal. In the acoustic case, the system (2) reduces to three identical Helmholtz equations in $\sigma_{ii},\ i = 1, 2, 3$. We test our scheme for both the elastic and acoustic cases. For the elastic case, we impose Dirichlet boundary conditions (BC) determined by Pilant's solution [23, §7.4]. For the acoustic case ($c_s = 0$), we use the high-order gradient absorbing boundary condition (ABC) developed in [11], as well as Dirichlet BC based on the Green's function solution to the Helmholtz equation. In the elastic case, the fourth order scheme shows a significant improvement over the second order scheme at different grid sizes.

In our tests, we assume that the forcing function has a small finite support. This is a situation that occurs in many real physical cases, such as explosions, earthquakes and volcano eruptions. It also occurs in geophysical prospecting, in which point-wise impacts are created at many points, and many detectors measure the resulting reverberations. The frequency-domain implementation of one important reconstruction method, known as "full waveform inversion" (FWI) involves the repeated numerical solution of the Helmholtz equation or the elastic wave equation; see Virieux and Operto [33], Kallivokas et al. [15], van Leeuwen and Herrmann [31] and Fathi et al. [5].

Three major issues affect the accuracy of the solution obtained by any numerical method: the accuracy of the interior scheme used, the accuracy of the solver, and the absorbing boundary conditions. The ability to handle variable wave speeds is essential for many applications in which the domain is heterogeneous. For the solver of the elastic equation, we use the CARP-CG algorithm [9], which was very useful for solving the Helmholtz equation at high frequencies [10, 11, 30] and for the elastic wave equation [19, 20]. For the elastic equation, we do not use any absorbing boundary conditions, as our purpose is to test the accuracy of the compact fourth order scheme. Instead we compare our numerical results with Pilant's solution [23, §7.4], with very favorable results. We also obtain a very significant improvement over the second order scheme.

The rest of the paper is organized as follows: Section 2 presents the discretization, Section 3 provides the implementation details. Section 4 presents experimental results on a model with a known analytic solution, for both the acoustic and elastic cases. We conclude with Section 5.

2 Discretization of the elastic wave equation

We shall now develop a compact fourth order scheme for the first order formulation of the elastic wave equation. Using a Taylor series expansion, we have (ignore j and k indices):

$$\begin{aligned}
\delta_x u &\equiv \frac{u_{i+1} - u_{i-1}}{2h} = u_x + \frac{h^2}{6} u_{xxx} + O(h^4) \\
\delta_{x/2} u &\equiv \frac{u_{i+1/2} - u_{i-1/2}}{h} = u_x + \frac{h^2}{24} u_{xxx} + O(h^4) \\
\delta_{xx} u &\equiv \frac{u_{i+1} - 2u_i + u_{i-1}}{h^2} = u_{xx} + \frac{h^2}{12} u_{xxxx} + O(h^4)
\end{aligned}$$

or

$$\begin{aligned}
u_x &= \delta_x u - \frac{h^2}{6} u_{xxx} + O(h^4) \\
u_x &= \delta_{x/2} u - \frac{h^2}{24} u_{xxx} + O(h^4) \\
u_{xx} &= \delta_{xx} u - \frac{h^2}{12} u_{xxxx} + O(h^4)
\end{aligned} \tag{4}$$

We can see from the two expressions for u_x that the coefficient of u_{xxx} in the staggered mesh is $h^2/24$, which is one fourth of the coefficient of u_{xxx} in a regular mesh. This means that the truncation error of the staggered mesh is one fourth of that on the non-staggered mesh.

We also need on the boundary a one sided difference for a derivative. This is given by

$$u_x = \frac{-3u_i + 4u_{i+1} - u_{i+2}}{2h} + \frac{h^2}{3} u_{xxx} + O(h^4). \tag{5}$$

For details regarding the development of the the above equations, see [29]. In order to deal with both a staggered and nonstaggered grid in the same derivation we shall use the notation

$$u_x = \delta_x u - \alpha h^2 u_{xxx} + O(h^4) \tag{6}$$

where $\alpha = 1/6$ or $1/24$ for a nonstaggered or staggered grid, respectively.

For a nonstaggered grid we use the neighbors $i-1, i+1$, while for a staggered grid we use the following locations of the variables on an $h \times h \times h$ cube of grid points:

$\sigma_{11}, \sigma_{22}, \sigma_{33} \rightarrow (i, j, k)$

$u \rightarrow (i + 1/2, j, k) \quad v \rightarrow (i, j + 1/2, k) \quad w \rightarrow (i, j, k + 1/2)$

$\sigma_{12} \rightarrow (i + 1/2, j + 1/2, k) \quad \sigma_{13} \rightarrow (i + 1/2, j, k + 1/2) \quad \sigma_{23} \rightarrow (i, j + 1/2, k + 1/2)$

Our staggered grid implementation is described visually by Fig. 1, which shows the positions of the nine variables.

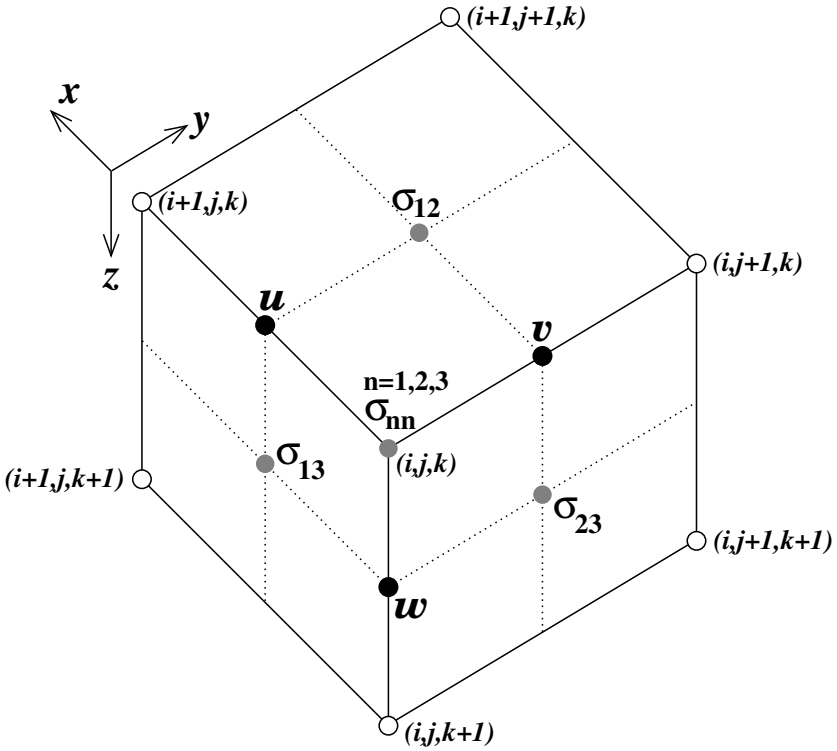

Figure 1: The compact 4th order scheme on a staggered grid, showing the positions of the 9 variables on an $h \times h \times h$ cube. $\sigma_{11}, \sigma_{22}, \sigma_{33}$ are located at a grid point (i, j, k), u is located at $(i+1/2, j, k)$, v is at $(i, j+1/2, k)$, and w is at $(i, j, k+1/2)$. σ_{12} is at $(i+1/2, j+1/2, k)$, σ_{13} is at $(i+1/2, j, k+1/2)$, and σ_{23} is at $(i, j+1/2, k+1/2)$.

We discretize Eq. (2), in frequency space, where λ and μ may vary in space. We then get:

$$
\begin{aligned}
-\rho i\omega u &= \delta_x \sigma_{11} + \delta_y \sigma_{12} + \delta_z \sigma_{13} + F^u \\
&\quad - \alpha h^2 \left((\sigma_{11})_{xxx} + (\sigma_{12})_{yyy} + (\sigma_{13})_{zzz} \right) + O(h^4) && \text{(7a)} \\
-\rho i\omega v &= \delta_x \sigma_{12} + \delta_y \sigma_{22} + \delta_z \sigma_{23} + F^v \\
&\quad - \alpha h^2 \left((\sigma_{12})_{xxx} + (\sigma_{22})_{yyy} + (\sigma_{23})_{zzz} \right) + O(h^4) && \text{(7b)} \\
-\rho i\omega w &= \delta_x \sigma_{13} + \delta_y \sigma_{23} + \delta_z \sigma_{33} + F^w \\
&\quad - \alpha h^2 \left((\sigma_{13})_{xxx} + (\sigma_{23})_{yyy} + (\sigma_{33})_{zzz} \right) + O(h^4) && \text{(7c)} \\
-i\omega \sigma_{11} &= (\lambda + 2\mu)\delta_x u + \lambda(\delta_y v + \delta_z w) \\
&\quad - \alpha h^2 \left((\lambda + 2\mu) u_{xxx} + \lambda(v_{yyy} + w_{zzz}) \right) + O(h^4) && \text{(7d)} \\
-i\omega \sigma_{22} &= (\lambda + 2\mu)\delta_y v + \lambda(\delta_x u + \delta_z w) \\
&\quad - \alpha h^2 \left((\lambda + 2\mu) v_{yyy} + \lambda(u_{xxx} + w_{zzz}) \right) + O(h^4) && \text{(7e)} \\
-i\omega \sigma_{33} &= (\lambda + 2\mu)\delta_z w + \lambda(\delta_x u + \delta_y v)
\end{aligned}
$$

$$- \alpha h^2 \left((\lambda + 2\mu) w_{zzz} + \lambda (u_{xxx} + v_{yyy}) \right) + O(h^4) \tag{7f}$$

$$-i\omega\sigma_{12} = \mu(\delta_y u + \delta_x v) - \alpha h^2 \mu (u_{yyy} + v_{xxx}) + O(h^4) \tag{7g}$$

$$-i\omega\sigma_{13} = \mu(\delta_z u + \delta_x w) - \alpha h^2 \mu (u_{zzz} + w_{xxx}) + O(h^4) \tag{7h}$$

$$-i\omega\sigma_{23} = \mu(\delta_z v + \delta_y w) - \alpha h^2 \mu (v_{zzz} + w_{yyy}) + O(h^4) \tag{7i}$$

We need to eliminate terms with the subscripts xxx, yyy, zzz from equations (7) since these cannot be approximated to 4th order on a compact stencil. This will be done with the aid of equations (2). Starting with equations (7a)–(7c), we differentiate (2a) with respect to xx and get

$$-i\omega(\rho u)_{xx} = \frac{\partial^3 \sigma_{11}}{\partial x^3} + \frac{\partial^3 \sigma_{12}}{\partial x^2 \partial y} + \frac{\partial^3 \sigma_{13}}{\partial x^2 \partial z} + F^u_{xx} \tag{8}$$

or

$$\frac{\partial^3 \sigma_{11}}{\partial x^3} = -\left[\frac{\partial^3 \sigma_{12}}{\partial x^2 \partial y} + \frac{\partial^3 \sigma_{13}}{\partial x^2 \partial z} + i\omega(\rho u)_{xx} + F^u_{xx} \right] \tag{9}$$

Using a Taylor expansion, we have

$$\frac{\partial^3 \sigma_{11}}{\partial x^3} = -\Big[\delta_{xxy}\sigma_{12} + \delta_{xxz}\sigma_{13} + i\omega\delta_{xx}(\rho u) + \delta_{xx}F^u \Big] + O(h^2), \tag{10}$$

with similar expressions for $\frac{\partial^3 \sigma_{12}}{\partial y^3}$ and $\frac{\partial^3 \sigma_{13}}{\partial z^3}$. For convenience, we define Δ_h as the second order approximation of the Laplacian, e.g., $\Delta_h F = (\delta_{xx} + \delta_{yy} + \delta_{zz})F + O(h^2)$. Substituting (10) and similar expressions back into (7a,7b,7c), we get

$$\begin{aligned}
-\rho i\omega u \;=\; & \delta_x\sigma_{11} + \delta_y\sigma_{12} + \delta_z\sigma_{13} + F^u \\
& + \alpha h^2 \Big[(\delta_{xyy} + \delta_{xzz})\sigma_{11} + (\delta_{xxy} + \delta_{yzz})\sigma_{12} + (\delta_{xxz} + \delta_{yyz})\sigma_{13} \\
& + i\omega\Delta_h(\rho u) + \Delta_h F^u \Big] + O(h^4)
\end{aligned} \tag{11a}$$

$$\begin{aligned}
-\rho i\omega v \;=\; & \delta_x\sigma_{21} + \delta_y\sigma_{22} + \delta_z\sigma_{23} + F^v \\
& + \alpha h^2 \Big[(\delta_{xyy} + \delta_{xzz})\sigma_{21} + (\delta_{xxy} + \delta_{yzz})\sigma_{22} + (\delta_{xxz} + \delta_{yyz})\sigma_{23} \\
& + i\omega\Delta_h(\rho v) + \Delta_h F^v \Big] + O(h^4)
\end{aligned} \tag{11b}$$

$$\begin{aligned}
-\rho i\omega w \;=\; & \delta_x\sigma_{31} + \delta_y\sigma_{32} + \delta_z\sigma_{33} + F^w \\
& + \alpha h^2 \Big[(\delta_{xyy} + \delta_{xzz})\sigma_{31} + (\delta_{xxy} + \delta_{yzz})\sigma_{32} + (\delta_{xxz} + \delta_{yyz})\sigma_{33} \\
& + i\omega\Delta_h(\rho w) + \Delta_h F^w \Big] + O(h^4)
\end{aligned} \tag{11c}$$

Since we have at most 2 differences in any direction, this is defined on the compact stencil. For the stress equations the formulae are more complicated when the parameters ρ, λ and μ are functions of x, y, z. We assume λ and μ are explicitly known functions of the space variables.

We now follow a similar procedure with the stress equations (7d)–(7i). To eliminate the third order derivatives w.r.t. to a single variable in (7d)–(7i), we rewrite the relevant equation from

(2d)–(2f) and differentiate twice. For example, we rewrite (2d) as

$$u_x = -i\omega \frac{\sigma_{11}}{\lambda + 2\mu} - \frac{\lambda v_y}{\lambda + 2\mu} - \frac{\lambda w_z}{\lambda + 2\mu}$$

and differentiate twice w.r.t. x to get:

$$u_{xxx} = -i\omega \left(\frac{\sigma_{11}}{\lambda + 2\mu} \right)_{xx} - \left(\frac{\lambda v_y}{\lambda + 2\mu} \right)_{xx} - \left(\frac{\lambda w_z}{\lambda + 2\mu} \right)_{xx} \tag{12}$$

Similarly, from (2d) we also have

$$v_y = -i\omega \frac{\sigma_{11}}{\lambda} - \frac{(\lambda + 2\mu)}{\lambda} u_x - w_z$$

Differentiating twice w.r.t. y we get:

$$v_{yyy} = -i\omega \left(\frac{\sigma_{11}}{\lambda} \right)_{yy} - \left(\frac{\lambda + 2\mu}{\lambda} u_x \right)_{yy} - w_{yyz} \tag{13}$$

and again from (2d) we also get

$$w_{zzz} = -i\omega \left(\frac{\sigma_{11}}{\lambda} \right)_{zz} - \left(\frac{\lambda + 2\mu}{\lambda} u_x \right)_{zz} - v_{yzz} \tag{14}$$

This is then used to replace the $O(h^2)$ term on the right hand side of (7d). Note that we have expressed $u_{xxx}, v_{yyy}, w_{zzz}$ in terms of σ_{11} and its derivatives, and so the modified version of (7d) will involve only σ_{11} and u, v, w and their mixed derivatives.

We now repeat this procedure with equations (2e) and (2f), and modify the remaining equations (7e) to (7i). Finally, substituting these expressions into Equations (7d) to (7i), we get

$$\begin{aligned}
-i\omega\sigma_{11} &= (\lambda + 2\mu)\delta_x u + \lambda(\delta_y v + \delta_z w) \qquad (15a)\\
&\quad + \alpha h^2 \left[i\omega \left((\lambda + 2\mu) \Big(\frac{\sigma_{11}}{\lambda + 2\mu} \Big)_{xx} + \lambda \left(\Big(\frac{\sigma_{11}}{\lambda} \Big)_{yy} + \Big(\frac{\sigma_{11}}{\lambda} \Big)_{zz} \right) \right) \right.\\
&\quad + (\lambda + 2\mu) \Big(\frac{\lambda}{\lambda + 2\mu} (v_y + w_z) \Big)_{xx}\\
&\quad \left. + \lambda \left(\Big(\frac{\lambda + 2\mu}{\lambda} u_x \Big)_{yy} + \Big(\frac{\lambda + 2\mu}{\lambda} u_x \Big)_{zz} + v_{yzz} + w_{yyz} \right) \right] + O(h^4)\\
-i\omega\sigma_{22} &= (\lambda + 2\mu)\delta_y v + \lambda(\delta_x u + \delta_z w) \qquad (15b)\\
&\quad + \alpha h^2 \left[i\omega \left((\lambda + 2\mu) \Big(\frac{\sigma_{22}}{\lambda + 2\mu} \Big)_{yy} + \lambda \left(\Big(\frac{\sigma_{22}}{\lambda} \Big)_{xx} + \Big(\frac{\sigma_{22}}{\lambda} \Big)_{zz} \right) \right) \right.\\
&\quad + (\lambda + 2\mu) \Big(\frac{\lambda}{\lambda + 2\mu} (u_x + w_z) \Big)_{yy}\\
&\quad \left. + \lambda \left(\Big(\frac{\lambda + 2\mu}{\lambda} v_y \Big)_{xx} + \Big(\frac{\lambda + 2\mu}{\lambda} v_y \Big)_{zz} + u_{xzz} + w_{xxz} \right) \right] + O(h^4)
\end{aligned}$$

$$
\begin{aligned}
-i\omega\sigma_{33} &= (\lambda+2\mu)\delta_z w + \lambda(\delta_x u + \delta_y v) \qquad (15c)\\
&\quad + \alpha h^2 \left[i\omega \left((\lambda+2\mu)\Big(\frac{\sigma_{33}}{\lambda+2\mu}\Big)_{zz} + \lambda\left(\Big(\frac{\sigma_{33}}{\lambda}\Big)_{xx} + \Big(\frac{\sigma_{33}}{\lambda}\Big)_{yy}\right)\right)\right.\\
&\quad + (\lambda+2\mu)\Big(\frac{\lambda}{\lambda+2\mu}(u_x+v_y)\Big)_{zz}\\
&\quad \left. + \lambda\left(\Big(\frac{\lambda+2\mu}{\lambda}w_z\Big)_{xx} + \Big(\frac{\lambda+2\mu}{\lambda}w_z\Big)_{yy} + u_{xyy} + v_{xxy}\right)\right] + O(h^4)\\
-i\omega\frac{1}{\mu}\sigma_{12} &= \delta_y u + \delta_x v \qquad (15d)\\
&\quad + \alpha h^2 \left[i\omega\left(\Big(\frac{1}{\mu}\sigma_{12}\Big)_{xx} + \Big(\frac{1}{\mu}\sigma_{12}\Big)_{yy}\right) + u_{xxy} + v_{xyy}\right] + O(h^4)\\
-i\omega\frac{1}{\mu}\sigma_{13} &= \delta_z u + \delta_x w \qquad (15e)\\
&\quad + \alpha h^2 \left[i\omega\left(\Big(\frac{1}{\mu}\sigma_{13}\Big)_{xx} + \Big(\frac{1}{\mu}\sigma_{13}\Big)_{zz}\right) + u_{xxz} + w_{xzz}\right] + O(h^4)\\
-i\omega\frac{1}{\mu}\sigma_{23} &= \delta_z v + \delta_y w + \qquad (15f)\\
&\quad + \alpha h^2 \left[i\omega\left(\Big(\frac{1}{\mu}\sigma_{23}\Big)_{yy} + \Big(\frac{1}{\mu}\sigma_{23}\Big)_{zz}\right) + v_{yyz} + w_{yzz}\right] + O(h^4)
\end{aligned}
$$

The derivatives in the $O(h^2)$ terms are all replaced by second order central differences. Since these are all mixed derivatives they can be computed on the compact stencil. At a boundary, we specify Dirichlet boundary conditions based on Pilant's solution (see next section).

3 Implementation details

3.1 The Acoustic case

This case is obtained when $c_s = 0$ (see Eq. (3a)), from which it follows that $\mu = 0$ and $\lambda = \rho c_p^2$. Setting $\mu = 0$ in Eq. (2), we get:

$$
\begin{aligned}
\sigma_{ij} &= 0 \text{ for } i \neq j\\
\sigma \triangleq \sigma_{11} &= \sigma_{22} = \sigma_{33} = \frac{-\lambda}{i\rho\omega}(u_x + v_y + w_z)\\
\sigma_x &= -i\rho\omega u - F^u\\
\sigma_y &= -i\rho\omega v - F^v\\
\sigma_z &= -i\rho\omega w - F^w\\
\therefore\ \ \sigma_{xx} + \sigma_{yy} + \sigma_{zz} &= -i\rho\omega(u_x + v_y + w_z) - F\\
&= -i\rho\omega\,\frac{i\rho\omega}{-\lambda}\,\sigma - F,
\end{aligned}
$$

$$\text{where } F = F_x^u + F_y^v + F_z^w$$

$$\therefore \quad \Delta\,\sigma + \frac{\rho^2\omega^2}{\lambda}\,\sigma = -F. \tag{16a}$$

Eq. (16a) is the Helmholtz equation with the wavenumber $k = \dfrac{\rho\omega}{\sqrt{\lambda}}$. The Green's function solution to this equation in n-dimensional space is the convolution

$$\sigma(\boldsymbol{x}) \;=\; \int_{\mathbb{R}^n} G(\boldsymbol{x}-\boldsymbol{y})F(\boldsymbol{y})d\boldsymbol{y}, \tag{17}$$

where $\boldsymbol{x}$ and $\boldsymbol{y}$ are points in $\mathbb{R}^n$ and G is the Green's function for $\mathbb{R}^n$. In 3D, G is the following function:

$$G(\boldsymbol{x}) \;=\; \frac{e^{ik\|\boldsymbol{x}\|}}{4\pi\|\boldsymbol{x}\|}. \tag{18}$$

For the acoustic case, we assume that the impact function F is the delta function at the point of impact, so the integral in Eq. (17) reduces to the Green's function $G(\boldsymbol{x})$ (Eq. (18)).

For the boundary conditions, we added an extra layer of grid points on all sides of the domain. We used two types of boundary conditions (BC): Dirichlet BC based on the Green function, and absorbing boundary conditions (ABC) according to the "gradient method" introduced by the authors in [11]. The gradient ABC was implemented by using both the extra layer and the outermost layer of the original domain.

The "gradient method" (GM) is based on Sommerfeld's radiation condition [27, §28]:

$$\lim_{r\to\infty} r\left(\frac{\partial u}{\partial \boldsymbol{r}} - iku\right) = 0\,, \tag{19}$$

where u is the wavefield, r is the distance from a point source, $\boldsymbol{r}$ is unit vector pointing away from the source, and $\frac{\partial u}{\partial \boldsymbol{r}}$ is the directional derivative of u in the radial direction. Note that in this case, $\frac{\partial u}{\partial \boldsymbol{r}} = \boldsymbol{\nabla} u$, where $\boldsymbol{\nabla} u$ is the gradient of u. This led us in [11] to realize that in absorbing boundary conditions, at any point p on the boundary, directional derivatives of u should be taken in the direction of $\boldsymbol{\nabla} u$ at p, regardless of the orientation of the boundary at p. We called this approach the "Gradient Method" (GM).

An example of the application of GM to the Engquist-Majda (EM) is the following. The first order EM is $u_{\boldsymbol{n}} - iku = 0$, where $\boldsymbol{n}$ is the outward pointing normal to the boundary. The application of GM to EM consists of changing $\boldsymbol{n}$ to $\boldsymbol{g}$, where $\boldsymbol{g}$ is the unit vector in the direction of the gradient of u at the boundary point. This gives us $u_{\boldsymbol{g}} - iku = 0$ as the equivalent GM boundary condition.

Bayliss, Gunzberger and Turkel [1] developed a sequence of ABCs of increasing order. The first order ABC of the series, called BGT1, is the following:

$$\frac{\partial u}{\partial \boldsymbol{r}} + \left(\frac{1}{r} - ik\right) u = 0, \tag{20}$$

where r and $\boldsymbol{r}$ are the same as in (19). BGT was originally developed for a spherical domain with a point of impact at the center, so $\boldsymbol{r}$ is also the gradient of u at the boundary. Hence, according to the GM principle, the BGT ABCs can be used in any convex-shaped domain, with the point of impact at any interior point.

For the acoustic case, we used the second order BGT, which is the following:

$$\text{BGT2: } u_{\boldsymbol{rr}} + \alpha(r)u_{\boldsymbol{r}} + \beta(r)u = 0, \tag{21}$$

where

$$\alpha(r) = \left(\frac{4}{r} - 2ik\right) \text{ and } \beta(r) = \left(\frac{2}{r^2} - k^2 - \frac{4ik}{r}\right).$$

3.2 The elastic case

Pilant's solution. Pilant [23, §7.4] (see case "Elastic Media – Point Force") developed an exact solution for the 3D case with a one-directional single point source of impact. Pilant's solution for an impact force in the z-direction (see [23, Eq. 7-88]) is

$$\mathbf{W} = \frac{-F(\omega)}{4\pi\rho\omega^2}\left[\nabla\nabla\Big(\frac{e^{ik_pR}}{R}\mathbf{e}_z - \frac{e^{ik_sR}}{R}\mathbf{e}_z\Big) - k_s^2\frac{e^{ik_pR}}{R}\mathbf{e}_z\right], \tag{22}$$

where $\mathbf{W} = (u, v, w)$, $\mathbf{e}_z$ is the unit vector in the z direction (the direction of the impact), R is the distance from the source of impact, $F(\omega) = \int_{-\infty}^{\infty} f(t)e^{i\omega t}dt$, where $f(t)$ is the force of impact in the z direction at time t. We also assume this type of point source of impact, so in the terminology of this paper, Pilant's $F(\omega)$ is our $F^w(x_0, y_0, z_0)$, where (x_0, y_0, z_0) is the point source of impact. Note that since we assume that the force of impact is in the z direction, then the terms F^u and F^v of equations (2a) and (2b) are zero.

Eq. (22) was expanded in [12, Eq. 45] to the following expressions for the displacements:

$$u = \frac{F^w(x_0, y_0, z_0)}{4\pi\rho R^5\omega^2}xz\Big[(R^2k_p^2 - 3 - 3ik_pR)e^{-ik_pR} - (R^2k_s^2 - 3 - 3ik_sR)e^{-ik_sR}\Big] \tag{23a}$$

$$v = \frac{F^w(x_0, y_0, z_0)}{4\pi\rho R^5\omega}yz\Big[(R^2k_p^2 - 3 - 3ik_pR)e^{-ik_pR} - (R^2k_s^2 - 3 - 3ik_sR)e^{-ik_sR}\Big] \tag{23b}$$

$$\begin{aligned} w = \frac{F^w(x_0, y_0, z_0)}{4\pi\rho R^5\omega}\Big[&(x^2 + y^2 - 2z^2)(e^{-ik_pR} - e^{-ik_sR}) + \\ &\big(z^2R^2k_p^2 + i(x^2 + y^2 - 2z^2)Rk_p\big)\, e^{-ik_pR} + \\ &\big((x^2 + y^2)R^2k_s^2 - i(x^2 + y^2 - 2z^2)Rk_s\big)\, e^{-ik_sR}\Big] \end{aligned} \tag{23c}$$

As noted in [20, p. 1070], the displacements in (23) should be multiplied by $-i\omega$ in order to obtain the velocities. Clearly, $F^w(x_0, y_0, z_0)$ can be taken as a constant, which we assumed to

be 10^9. Our purpose in this paper is to test the accuracy of the compact fourth order scheme, so we applied Dirichlet boundary conditions taken from Pilant's solution – Eq. (23).

3.3 Solution methods

For the elastic case, we used the block-parallel CARP-CG algorithm [9]. In previous work, this algorithm was found to be very efficient on the Helmholtz equation with very high frequencies [10], convection-dominated PDEs [9], and in general, on linear systems with large off-diagonal elements and/or discontinuous coefficients [8]. CARP-CG is the parallel equivalent of the Björck and Elfving's CGMN algorithm [3]. It was also used in several previous works on elasticity; see [14, 19, 20]. The following is a brief outline of CARP-CG.

CARP-CG is a CG acceleration of CARP (component-averaged row projections) [7], which is a block-parallel extension of KACZ – the Kaczmarz algorithm [16]. KACZ is inherently sequential: starting from an arbitrary initial point, it sweeps through the equations by successively projecting the current iterate towards the hyperplane defined by the next equation. The extent of the projection is determined by the value of a relaxation parameter. It is well known that KACZ is SOR (successive over-relaxation) on the normal equations system $AA^Ty = b,\ x = A^T$. CARP divides the equations into blocks (which may overlap) and assigns each block to a processor. Every variable shared by several blocks is copied to all processors whose assigned block of equations contains that variable. The following two steps are then repeated until convergence:

- Operating in parallel, each processor executes a KACZ sweep on the equations of its assigned block. For each shared variable, the processor uses its copy of that variable.
- The new value of every shared variable is obtained by averaging all its copies, and it is then distributed to the processors which share it.

For PDE problems defined over some domain, CARP is actually a form of domain decomposition, with blocks corresponding to subdomains. This way, shared variables are limited to grid points at subdomain boundaries. It is shown in [7, 9] that in some superspace of the problem space, CARP is actually KACZ with cyclic relaxation parameters (i.e., each equation has its own fixed relaxation parameter). This provides a convenient theoretical proof of convergence, and enables the CG acceleration of CARP as follows: by running CARP in a double (forward and backward) sweep of the equations, one obtains a symmetric positive semi-definite iteration matrix B (even if the original matrix is nonsymmetric). Thus, CG can be applied to B to obtain CARP-CG. CARP-CG has also been implemented in the extensive PHIST solver toolkit [28].

For the acoustic case ($\mu = 0$), we found that GMRES [25], with a restart value of 20 (see explanation below), was more efficient than CARP-CG for frequencies 5, 10, and 20, and slightly less

efficient than CARP-CG for $f = 30$, so we used GMRES for all frequencies. The improved performance of CARP-CG at high frequencies is not surprising as it was already observed in [10].

Explanation of restarted GMRES: given a linear system $Ax = b$ and some initial estimate x_0, GMRES creates successively larger Krylov subspaces $K_n = span\{r_0, Ar_0, A^2r_0, \ldots, A^{n-1}r_0\}$, where $r_0 = b - Ax_0$. In order to avoid the space blowup created by GMRES, it is customary to stop the process after some number of iterations n, and restart GMRES with the solution estimate obtained after n iterations. This procedure is called GMRES(n), or GMRES with a restart of n.

4 Experimental results

4.1 Evaluation methodology

Our model is similar to the one used by Li et al. in [20], with some differences: the main difference is that our stencil is compact. Also, [20] uses a PML boundary condition, while we use Dirichlet BC based on Pilant's solution. We also assume a different number of grid points per side. Li et al. [20] introduce a method of optimizing a non-compact stencil and present profiles of the wave fields. Our approach concentrates on the new compact stencil, and besides wavefields, we also provide a global error comparison compared with Pilant's solution.

The domain consists of a 2000^3 meters cube, divided by a grid of 140^3 grid points. An extra grid point was added on each side for the BGT2 ABC (for the acoustic case) and the Dirichlet boundary condition (for the elastic case). The impact function was simulated by setting a cube of $8 \times 8 \times 8$ grid points at the center of the domain, and setting Dirichlet boundary condition on the outer surface of the cube, according to Eq. (23). For the acoustic case, we used the same cube to simulate the impact function by setting the Green's function on its boundaries. Note that according to the staggered grid method shown in Fig. 1, the Dirichlet boundary condition requires not only values on the outer surface of the small cube, but also values which are interior and at a distance of $h/2$ from the outer surface. The same applies to the Dirichlet boundary conditions on the outer boundary.

Other parameters were as follows:

- Wave speeds: elastic case — $c_p = 5000$ m/s, $c_s = 2500$ m/s;
  acoustic case — $c_p = 2500$ m/s, $c_s = 0$.
- Density: $\rho = 1000$ kg/m^3.
- The values of λ and μ are determined, in each case, from Eq. (3).
- Frequencies used in the experiments: $f = 5, 10, 20, 30$ Hz.

- Number of grid points per wavelength: there are two such numbers, N_p and N_s determined by c_p and c_s. $N_p = c_p N_x/(fL)$ and $N_s = c_s N_x/(fL)$, where N_x is number of grid points on each side, and $L = 2000$ meters.
- The position of the point of impact is at the center. In the acoustic case, the impact is a 3D delta function. In the elastic case, the impact is in the z-direction and its value is determined by $F^{\omega}(x_0, y_0, z_0)$, which we set at 10^9
- In this paper, we use the following definition of the relative error: let x^* be the vector of the true solution (as given by Pilant's solution in our case), and x' is a calculated solution after several iterations. Then, the relative error is defined as $\|x^* - x'\|/\|x^*\|$. In the tables of the following section, the relative error was evaluated with σ_{11} for the acoustic case and w for the elastic case.

There are extreme differences in the order of magnitude of the various variables, and these differences cause numerical difficulties. To reduce this problem, we followed the method used by He et al. [14, p. 7], in which the values of σ_{ij} are divided by the scaling factor ρc_p. After some experimenting, we found that the scaling factor $1.5\rho c_p$ produced better results. Note that the coefficients of the scaled σ_{ij} have to be multiplied by the same scaling factor. In the acoustic case, the impact function of the Helmholtz equation is taken as the delta function, so the values of the variables are very much smaller than those of the elastic case, but we still need to use the scaling factor $1.5\rho c_p$ (which is half the size of the factor in the elastic case) to avoid the numerical problems.

4.2 The acoustic case

Summary of this case: we used the GMRES algorithm [25] with a restart value of 20, and calculated the values of σ_{11} with two boundary conditions: Dirichlet boundary conditions based on the Green's function solution, and the Gradient Method ABC using BGT2 (21). Tests were ran with frequencies 5, 10, 20 and 30 Hz, and the results were checked at regular intervals.

Table 1 shows the relative error and the number of iterations required to reach the best relative error, for each frequency. It can be seen that the gradient ABC produced better results than the Dirichlet BC, and at significantly fewer iterations.

Figures 2–4 show plots of three values, taken at various lines parallel to the x-axis, at frequency $f = 20$. The red plot shows the Green's function solution, the green plot shows the solution with Dirichlet boundary conditions, and the black plot shows the solution with the gradient ABC (BGT2). The indices j and k are, respectively, the y and z values that determine the line. These figures also show that the gradient ABC produced better results than the Dirichlet BC.

Boundary condition	freq.:	$f=5$	$f=10$	$f=20$	$f=30$
Gradient ABC (BGT2)	rel-err	1.12E-3	3.89E-4	5.30E-4	2.07E-3
	no. it.	1500	1250	3000	3000
Dirichlet BC	rel-err	1.57E-3	1.01E-3	1.42E-3	1.29E-3
	no. it.	8000	8000	6000	10000

Table 1: Runtime results for the acoustic case at all tested frequencies, showing relative error of σ_{11} and number of iterations, for the two types of boundary conditions.

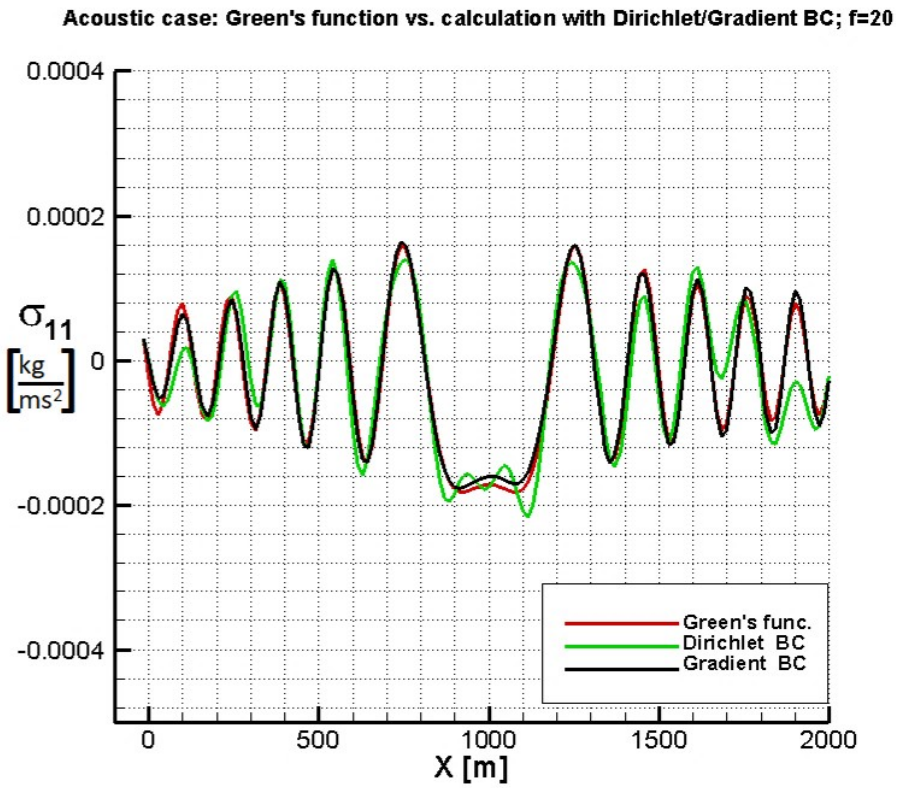

Figure 2: Acoustic case: $j=43, k=64$.

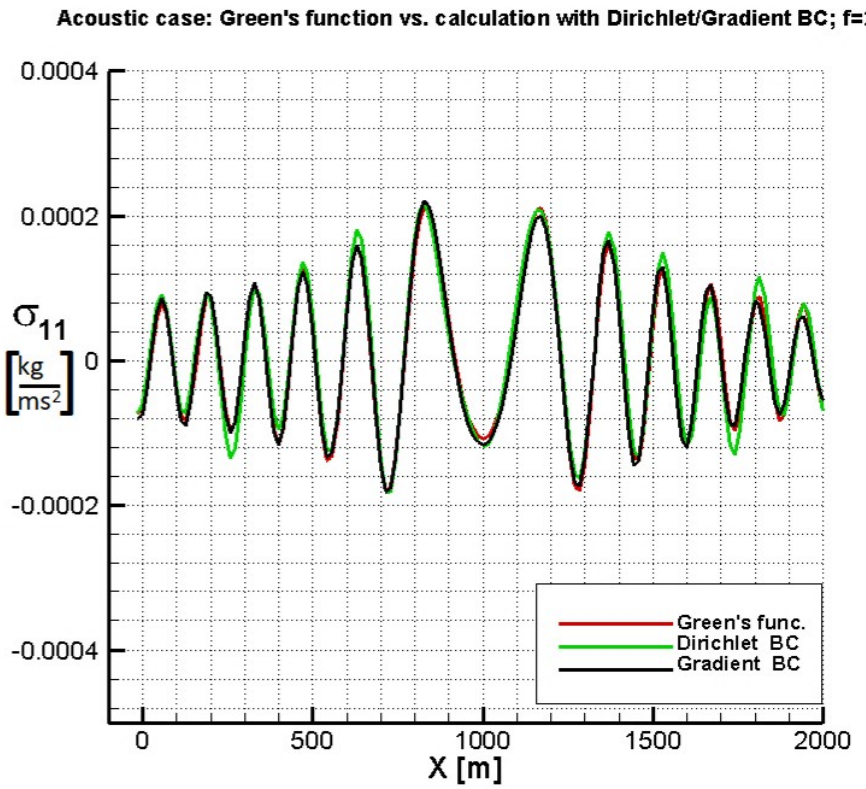

Figure 3: Acoustic case: $j = 50, k = 64$.

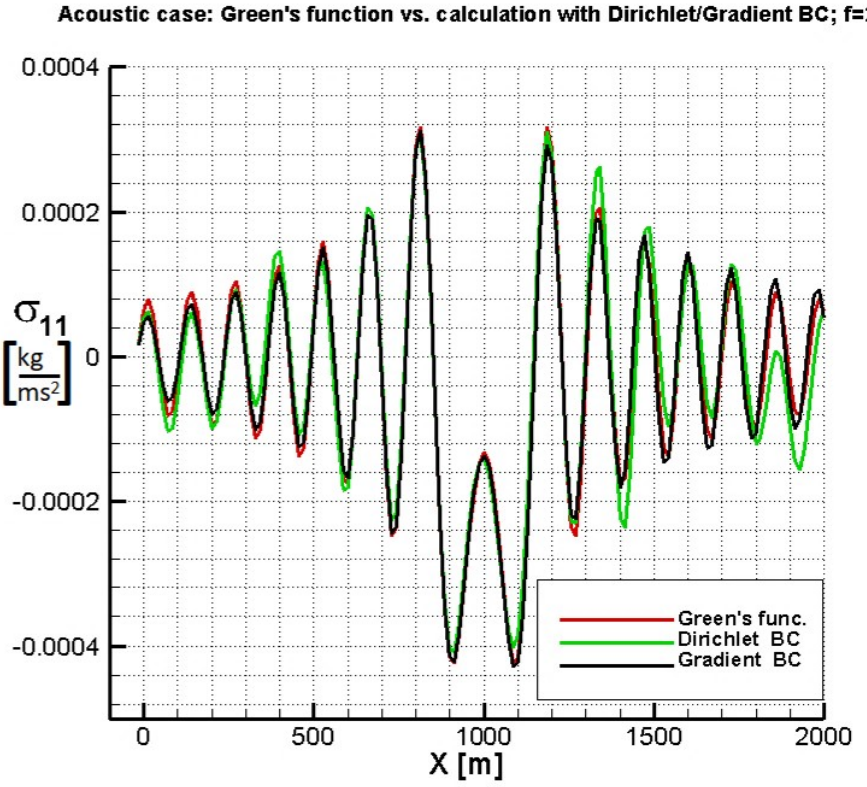

Figure 4: Acoustic case: $j = 64, k = 64$.

4.3 The elastic case

In this case, we used the CARP-CG algorithm [9], which produced much better results than GMRES in this case. We calculated the values of $u,\ v$ and w with Dirichlet boundary conditions based on Pilant's solution (23). Table 2 shows the best relative error results that were obtained for frequencies 5, 10, 20 and 30. Note that N_s is the number of grid points per wavelength – see Subsection 4.1. Also, the relative error in the following tables and figures is based only on the values of w.

frequency:	$f=5$	$f=10$	$f=20$	$f=30$
N_s	35	17.5	8.75	5.83
relative error	7.50E-3	2.74E-2	1.02E-1	2.41E-1

Table 2: Runtime results for the fourth-order elastic case at all tested frequencies on a grid of 140^3, showing relative error.

We now compare the relative errors obtained by the 2nd-order and 4th-order schemes for different grid sizes and frequencies. In this comparison, we let the program run until the relative error reached its lowest point. Tables 3 to 6, and corresponding Figures 5 to 8, show the results for frequencies $f=5$, $f=10$, $f\ =\ 20$ and $f=30$.

grid	70^3	80^3	90^3	100^3	110^3	120^3
N_s	17.50	20.00	22.50	25.00	27.50	30.00
2nd order	6.00E-2	5.52E-2	5.58E-2	5.46E-2	5.14E-2	4.71E-2
4th order	3.57E-2	3.27E-2	3.26E-2	1.42E-2	6.20E-3	4.20E-3

Table 3: Relative errors obtained with the 2nd- and 4th-order schemes for different grid sizes, for frequency $f=5$.

grid	70^3	80^3	90^3	100^3	110^3	120^3	130^3	140^3
N_s	8.75	10.00	11.25	12.50	13.75	15.00	16.25	17.50
2nd order	4.59E-1	3.78E-1	2.97E-1	2.35E-1	1.91E-1	1.52E-1	1.26E-1	1.10E-1
4th order	1.29E-1	1.21E-1	1.23E-1	1.06E-1	8.22E-2	5.37E-2	3.74E-2	2.74E-2

Table 4: Relative errors obtained with the 2nd- and 4th-order schemes for different grid sizes, for frequency $f=10$.

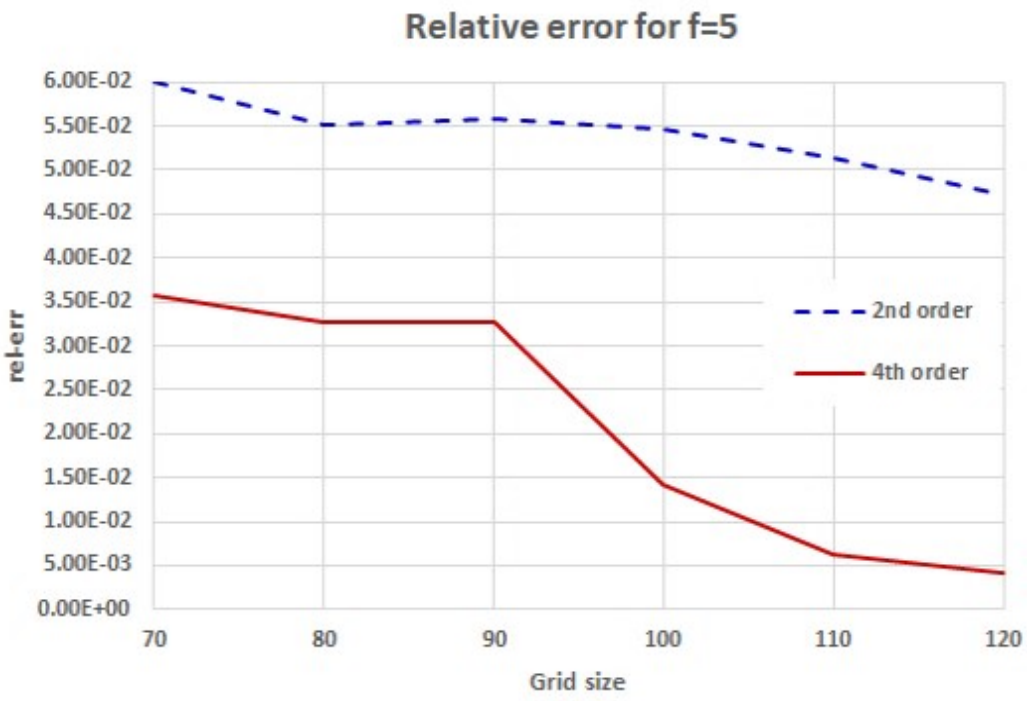

Figure 5: Plots of the relative error for different grid sizes, for the 2nd- and 4th-order schemes, for frequency $f = 5$.

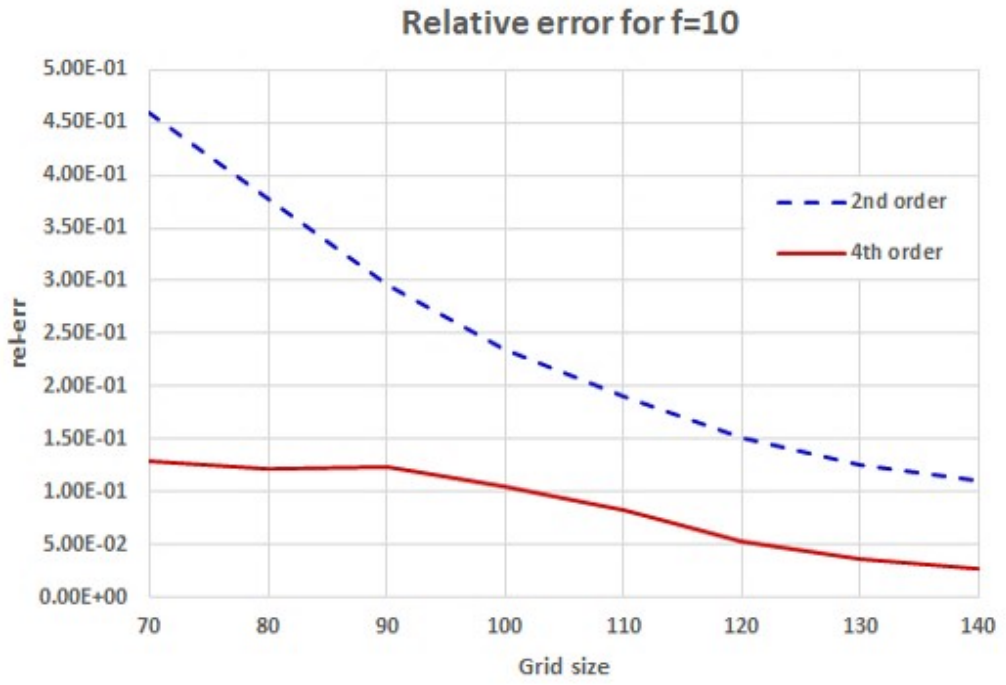

Figure 6: Plots of the relative error for different grid sizes, for the 2nd- and 4th-order schemes, for frequency $f = 10$.

grid	70^3	80^3	90^3	100^3	110^3	120^3	130^3	140^3	150^3	160^3
N_s	4.38	5.00	5.63	6.25	6.88	7.50	8.13	8.75	9.375	10
2nd order	8.42E-1	8.05E-1	6.64E-1	6.20E-1	6.47E-1	6.65E-1	6.55E-1	6.20E-1	5.71E-1	5.17E-1
4th order	3.27E-1	3.21E-1	2.31E-1	1.42E-1	1.02E-1	1.02E-1	1.02E-1	1.02E-1	9.40E-2	9.25E-2

Table 5: Relative errors obtained with the 2nd- and 4th-order schemes for different grid sizes, for frequency $f = 20$.

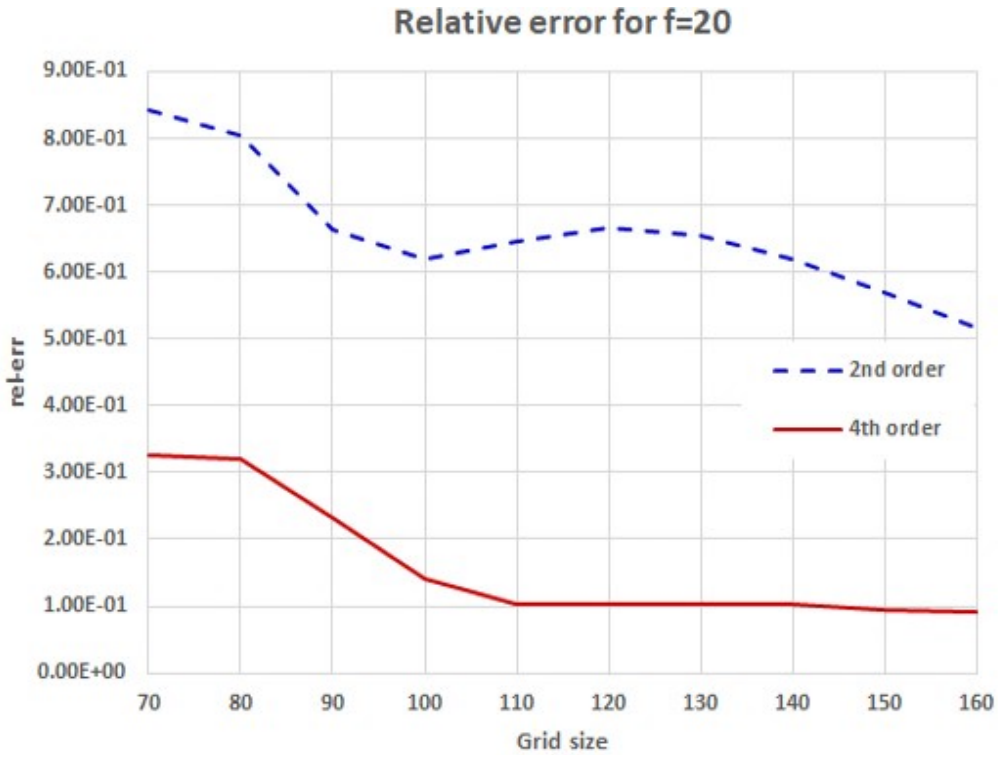

Figure 7: Plots of the relative error with different grid sizes, for the 2nd- and 4th-order schemes, for frequency $f = 20$.

grid	70^3	80^3	90^3	100^3	110^3	120^3	130^3	140^3	150^3	160^3
N_s	2.91	3.33	3.75	4.17	4.58	5.00	5.42	5.83	6.25	6.67
2nd order	9.96E-1	9.36E-1	9.65E-1	9.41E-1	9.14E-1	8.77E-1	8.11E-1	7.54E-1	7.35E-1	7.51E-1
4th order	7.63E-1	7.04E-1	5.23E-1	4.23E-1	4.34E-1	4.06E-1	3.25E-1	2.41E-1	1.74E-1	1.28E-1

Table 6: Relative errors obtained with the 2nd- and 4th-order schemes for different grid sizes, for frequency $f = 30$.

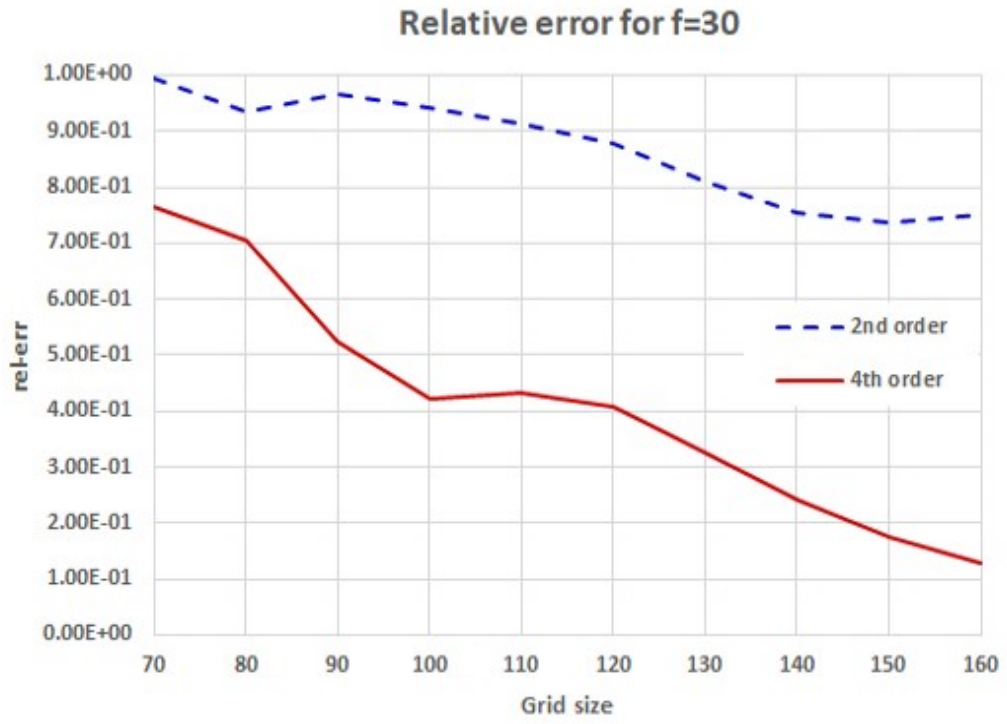

Figure 8: Plots of the relative error with different grid sizes, for the 2nd- and 4th-order schemes, for frequency $f = 30$.

These results show that the fourth order scheme is significantly better than the second order scheme. E.g., for $f = 10$, the accuracy obtained with the 2nd-order scheme with a grid of size 130^3 is achieved by the 4th-order scheme with a grid of size 70^3, which is only 15.6% of the 130^3-grid. Similar results can be seen for $f = 30$, but for $f = 5$ and $f = 20$, the 2nd-order scheme does not reach any of the results obtained by the 4th-order scheme (at the grid sizes that were tested). It can also be seen from the above tables that the most significant factor affecting the accuracy is the number of grid points per wavelength – N_s.

Figures 9–14 show plots of two values, taken at various lines parallel to the x-axis of the domain: Pilant's solution and the computational results obtained with Dirichlet boundary condition (based on Pilant's solution). The indices j and k are, respectively, the y and z values that determine the line. Note that the first two plots show the values of u, and the others show the values of w. The computational results show a good agreement with Pilant's solution, with a small exception at the center of Figure 11.

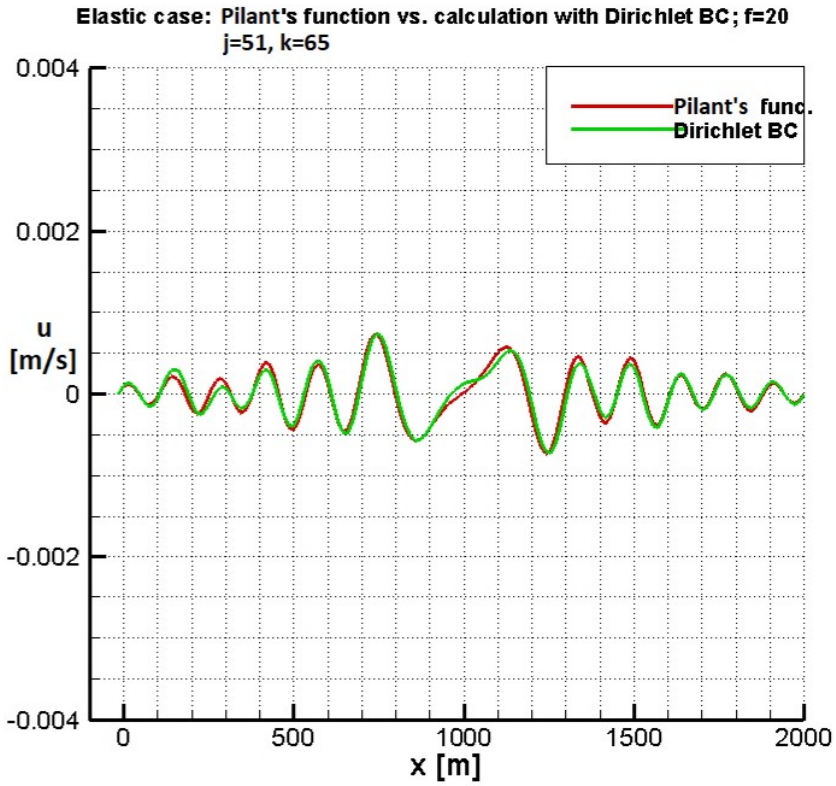

Figure 9: elastic case for u: $j=51, k=65$.

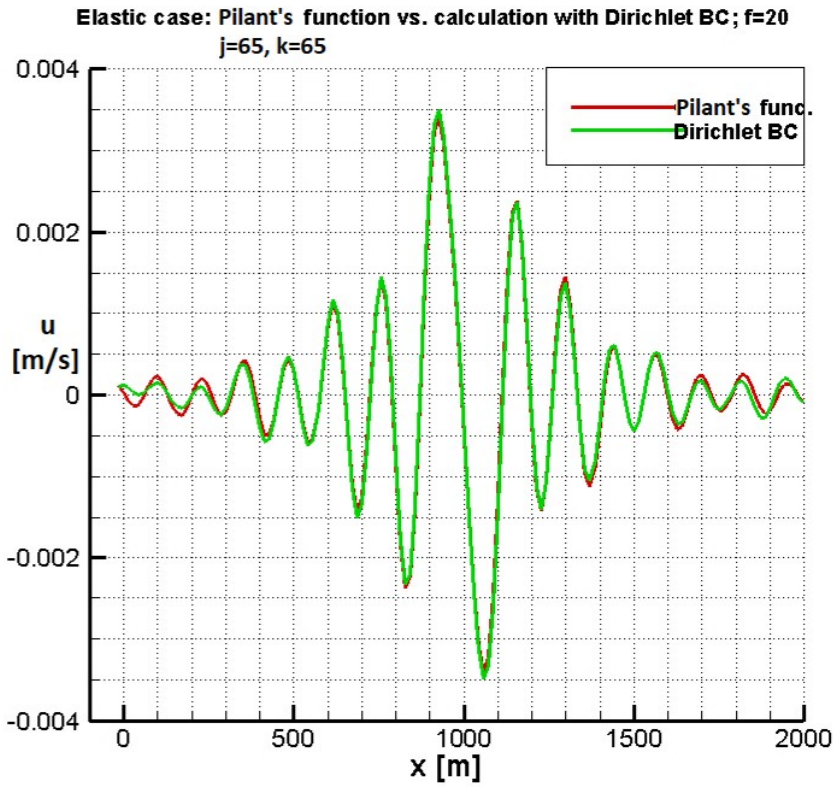

Figure 10: elastic case for u: $j=65, k=65$.

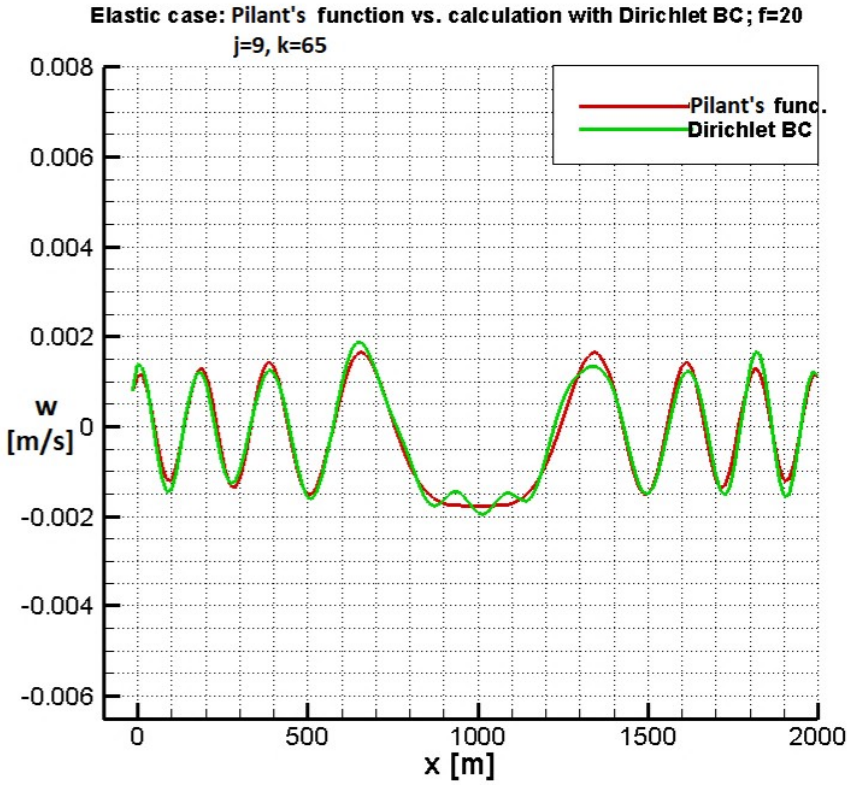

Figure 11: elastic case for w: $j=9, k=65$.

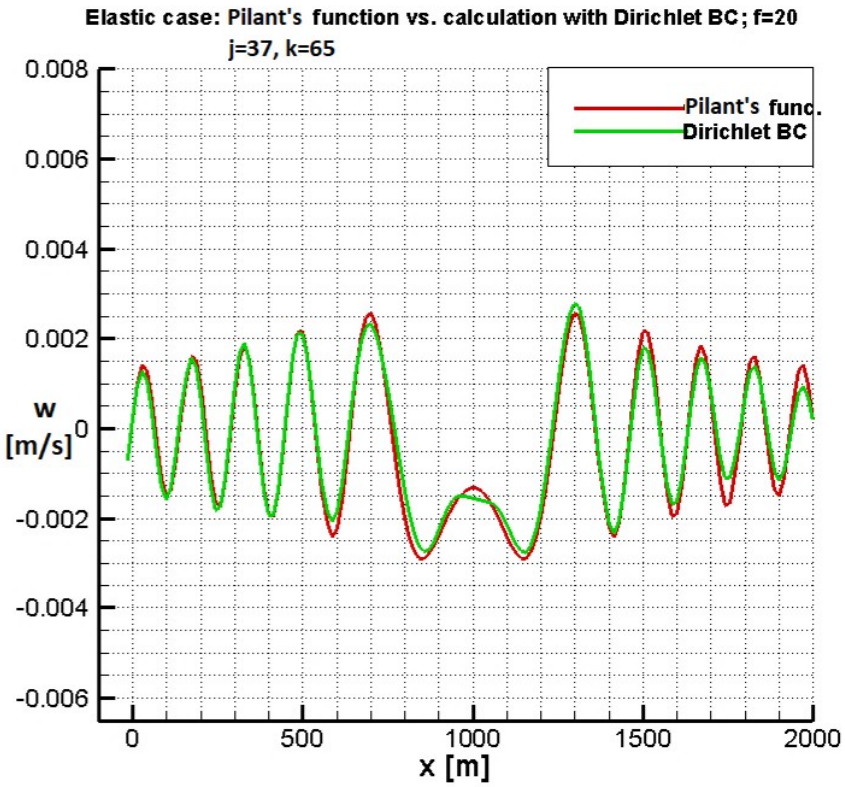

Figure 12: elastic case for w: $j=37, k=65$.

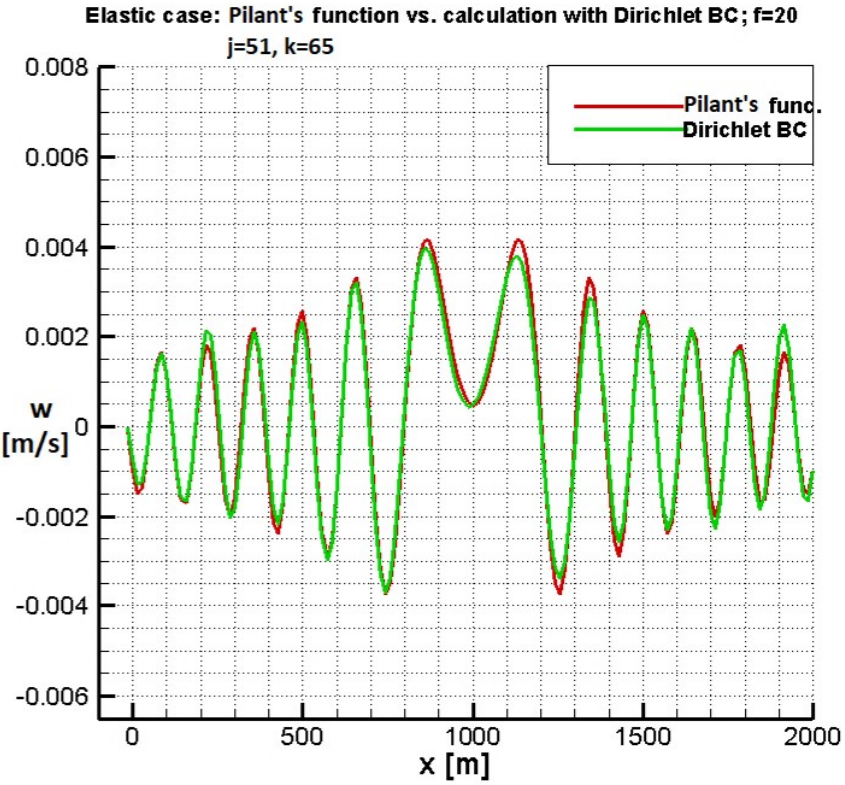

Figure 13: elastic case for w: $j=51, k=65$.

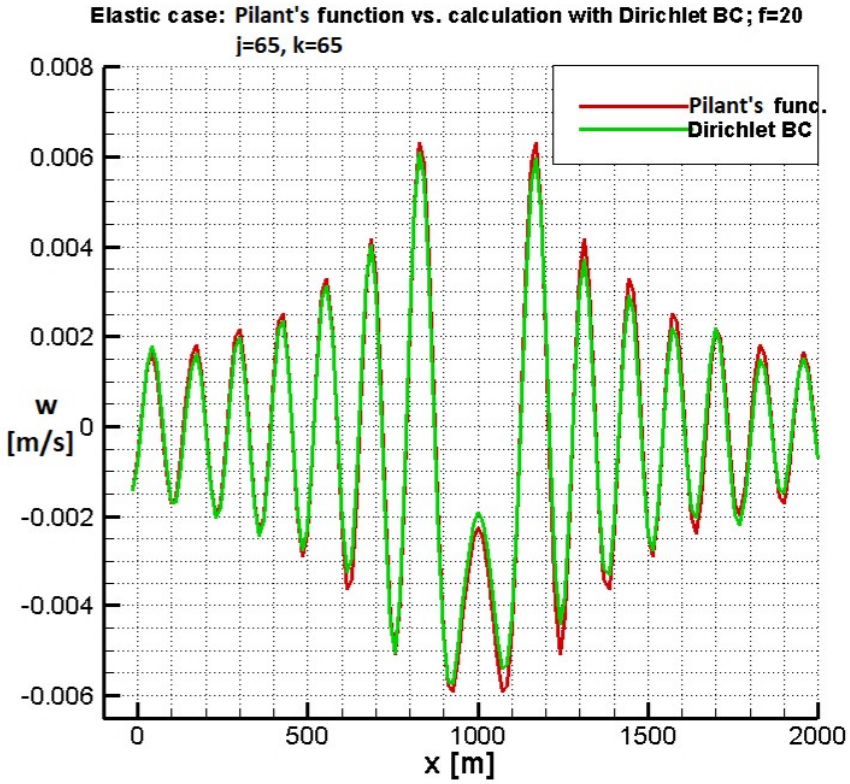

Figure 14: elastic case for w: $j = 65, k = 65$.

5 Conclusions

We presented a compact fourth order scheme for the elastic wave equation in the frequency domain, using the first order velocity-stress formulation. The new scheme was discretized on a staggered grid, assuming a homogeneous medium. We presented results for both the acoustic and the elastic cases. For the boundary conditions of the acoustic case, we used both the Dirichlet BC and the second order BGT boundary condition of [1] (which is also suitable for any convex domain according to the Gradient Method of [11]); the BGT boundary condition provided better computational results and at fewer iterations.

For the elastic case, we used Dirichlet BC based on Pilant's solution [23, §7.4] and expanded in [12, 20]. We showed that the fourth order scheme shows good agreement with Pilant's solution and provides significantly better results than the second order scheme.

Future work on this topic should implement our scheme for heterogeneous media, compare its performance with non-compact fourth order schemes, and test its performance on various geophysical models, using PML boundary conditions. Another topic would be to implement the optimization introduced in [20] to our scheme.

Acknowledgments. The authors wish to thank the reviewers for their detailed and helpful comments.

Data Availability Statement. Data available on request from the authors.

References

[1] A. Bayliss, M. Gunzburger and E. Turkel. Boundary conditions for the numerical solution of elliptic equations in exterior regions. *SIAM J. of Applied Mathematics* 42:430–451, 1982.

[2] A. Bayliss, C.I. Goldstein and E. Turkel. On Accuracy conditions for the numerical computation of waves. *J. of Computational Physics* 59:396-404, 1985.

[3] Å. Björck and T. Elfving. Accelerated projection methods for computing pseudoinverse solutions of systems of linear equations. *BIT* 19:145–163, 1979.

[4] A. Deraemaeker, I. Babuška and P. Bouillard. Dispersion and pollution of the FEM solution for the Helmholtz equation in one, two and three dimensions *International J. for Numerical Methods in Engineering* 46(4), 1999.

[5] A. Fathi, B. Poursartip, K.H. Stokoe II and L.F. Kallivokas. Three-dimensional P- and S-wave velocity profiling of geotechnical sites using full-waveform inversion driven by field data. *Soil Dynamics and Earthquake Engineering* 87:63–81, 2016.

[6] K.-A. Feng, C.-H. Teng, and M.-H. Chen. A pseudospectral penalty scheme for 2D isotropic elastic wave computations. *J. Sci. Comput.* 33:313—348, 2007.

[7] D. Gordon and R. Gordon. Component-averaged row projections: a robust, block-parallel scheme for sparse linear systems. *SIAM J. on Scientific Computing* 27:1092–1117, 2005.

[8] D. Gordon and R. Gordon. Solution methods for linear systems with large off-diagonal elements and discontinuous coefficients. *CMES-Computer Modeling in Engineering & Sciences* 53(1):23–45, 2009.

[9] D. Gordon and R. Gordon. CARP-CG: a robust and efficient parallel solver for linear systems, applied to strongly convection dominated PDEs. *Parallel Computing* 36:495–515, 2010.

[10] D. Gordon and R. Gordon. Parallel solution of high frequency Helmholtz equations using high order finite difference schemes. *Applied Mathematics & Computation* 218(21):10737–10754, 2012.

[11] D. Gordon, R. Gordon and E. Turkel. Compact high order schemes with gradient-direction derivatives for absorbing boundary conditions. *J. of Computational Physics* 297:295–315, 2015.

[12] B. Gosselin-Cliche and B. Giroux. 3D frequency-domain finite-difference viscoelastic-wave modeling using weighted average 27-point operators with optimal coefficients. *Geophysics* 79(3):T169–T188, 2014.

[13] R.W. Graves. Simulating seismic wave propagation in 3D elastic media using staggered-grid finite differences. *Bull. Seismol. Soc. Am.* 86:1091–1106, 1996.

[14] Q. He, B. Han, Y. Chen and Y. Li. Application of the finite-difference contrast source inversion method to multiparameter reconstruction using seismic full-waveform data. *J. of Applied Geophysics* 124:4–16, 2016.

[15] L.F. Kallivokas, A. Fathi, S. Kucukcoban, K.H. Stokoe II, J. Bielak and O. Ghattas. Site characterization using full waveform inversion. *Soil Dynamics and Earthquake Engineering* 47:62-82, 2013

[16] S. Kaczmarz. Angenäherte auflösung von systemen linearer gleichungen. *Bulletin de l'Académie Polonaise des Sciences et Lettres* A35:355–357, 1937.

[17] K. Komatitisch and J. Tromp. Introduction to the spectral element method for three-dimensional seismic wave propagation. *Geophys. J. Int.* 139:806–822, 1999.

[18] A.R. Levander. Fourth-order finite-difference P-SV seismograms. *Geophysics* 53:1425–1436, 1988.

[19] Y. Li, L. Métivier, R. Brossier, B. Han and J. Virieux. 2D and 3D frequency-domain elastic wave modeling in complex media with a parallel iterative solver. *Geophysics* 80(3):T101–T118, 2015.

[20] Y. Li, B. Han, L. Métivier and R. Brossier. Optimal fourth-order staggered-grid finite-difference scheme for 3D frequency-domain viscoelastic wave modeling. *J. of Computational Physics* 321:1055–1078, 2016.

[21] T. Ma and Y. Ge. High-order compact difference method for two-dimension elliptic and parabolic equations with mixed derivatives. *Tbilisi Math. J.* 13(4):141–167, 2020.

[22] S. Nilsson, N.A. Petersson, B. Sjögreen and H-O. Kreiss. Stable difference approximations for the elastic wave equation in second order formulation. *SIAM J. Numer. Anal.* 45:1902–1936, 2007.

[23] W.L. Pilant. *Elastic waves in the earth*. Vol. 11 in *Developments in Solid Earth Geophysics* Series, Elsevier, Holland, 1979.

[24] J. Pujol. *Elastic wave propagation and generation in seismology*. Cambridge University Press, Cambridge, UK, 2003

[25] Y. Saad and M.H. Schultz. GMRES: A generalized minimal residual algorithm for solving nonsymmetric linear systems. *SIAM J. Sci. Stat. Comput.* 7:856–869, 1986.

[26] B. Sjögreen and N.A. Petersson. A fourth order accurate finite difference scheme for the elastic wave equation in second order formulation *J. Sci. Comput.* 52:17–48, 2012.

[27] A. Sommerfeld. *Partial Differential Equations in Physics*, Academic Press, New York, 1964.

[28] J. Thies, M. Röhrig-Zöllner, N. Overmars, A. Basermann, D. Ernst, G. Hager and G. Wellein. PHIST: A pipelined, hybrid-parallel iterative solver toolkit. *ACM Trans. on Mathematical Software* 46(4), Oct. 2020.

[29] E. Turkel, High Order Methods, *Advances in Computational Electrodynamics: The Finite-Difference Time-Domain Method*, A. Taflove editor, Artech House, Boston, 63-109, 1998.

[30] E. Turkel, D. Gordon, R. Gordon and S. Tsynkov. Compact 2D and 3D sixth order schemes for the Helmholtz equation with variable wave number. *J. of Computational Physics* 232:272–287, 2013.

[31] T. van Leeuwen and F. Herrmann. 3D frequency-domain seismic inversion with controlled sloppiness. *SIAM J. on Scientific Computing* 36(5):S192–S217, 2014.

[32] J. Virieux. P-SV wave propagation in heterogeneous media: velocity-stress finite-difference method. *Geophysics* 51:889–901, 1986.

[33] J. Virieux and S. Operto. An overview of full-waveform inversion in exploration geophysics. *Geophysics* 74(6):wcc127–wcc152, 2009.

[34] J. Virieux et al., V. Etienne et al. and V. Cruz-Atienza et al. Modelling seismic wave propagation for geophysical imaging. *Earth and Planetary Sciences, Geology and Geophysics, "Seismic Waves - Research and Analysis*, chapter 13, Modelling Seismic Wave Propagation for Geophysical Imaging, edited by Masaki Kanao, 2012.